Hysteresis during Cycling of Nickel Hydroxide Active Material

Article *in* Journal of The Electrochemical Society · September 2001

DOI: 10.1149/1.1385846

3 authors, including:

John W Weidner
University of South Carolina
233 PUBLICATIONS **4,639** CITATIONS

SEE PROFILE

Journal of The Electrochemical Society, **148** (9) A969-A980 (2001)
0013-4651/2001/148(9)/A969/12/$7.00 © The Electrochemical Society, Inc.

Hysteresis during Cycling of Nickel Hydroxide Active Material

Venkat Srinivasan,[a,*,c] John W. Weidner,[a,*] and John Newman[b,]**

[a]*Department of Chemical Engineering, University of South Carolina, Columbia, South Carolina 29208, USA*
[b]*Department of Chemical Engineering, University of California, Berkeley, California 94720, USA*

The nickel hydroxide electrode is known to exhibit a stable hysteresis loop, with the potential on charge being higher than that on discharge at every state-of-charge (SOC). What we show here is that this loop created during a complete charge and discharge (*i.e.*, boundary curves) is not sufficient to define the state of the system. Rather, internal paths within the boundary curves (*i.e.*, scanning curves) can be generated that access potentials between the boundary curves. The potential obtained at any SOC, as well as how the material charges and discharges from that point, depends on the cycling history of the material. The implication of this phenomenon is that the potential of nickel-based batteries cannot be used as an indication of the SOC of the cell. Analysis of the boundary and scanning curves suggest that the electrode consists of a number of individual units or domains, each of which exhibits two or more metastable states. The cycling behavior of the nickel hydroxide electrode is discussed within the context of previously developed theoretical arguments regarding domain theory. Although the specific cause for the metastability in each domain is not understood, considerable insights are provided into the history-dependent behavior of the nickel hydroxide electrode. Finally, an empirical procedure is developed to predict the scanning curves based on the boundary curves.
 [DOI: 10.1149/1.1385846]

Manuscript submitted November 17, 2000; revised manuscript received April 23, 2001. Available electronically July 31, 2001.

Hysteresis is a characteristic of a system in which a change in the direction of the independent variable leads to the dependent variable failing to retrace the path it passed in the forward direction.[1] In other words, the dependent variable lags behind in an attempt to track the changes in the independent variable. Consequently, the system exhibits ''history dependence,'' with the path of the system dictated by its previous history. The phenomenon is manifested as a closed loop with two values of the dependent variable for each independent variable, one in the forward direction, and the other in the reverse. Most often, the size of the loop changes depending on the rate with which the independent variable is changed. A common electrochemical example of such a time-dependent hysteresis is cyclic voltammetry. The anodic and cathodic paths do not overlap due to kinetic, mass-transfer, and ohmic resistances, and therefore they move closer together as the rates are lowered. However, in a few systems, the loops generated are stable, reproducible, and rate-independent. Such loops are termed permanent hysteresis,[1] and they are the focus of this paper. From this point forward, the term hysteresis refers only to this rate-independent phenomenon.

Hysteresis is well-studied in adsorption[1] and magnetism,[2] but there are only a few documented examples in electrochemical systems. This includes the history-dependent equilibrium potential observed during the intercalation of lithium ions into carbon[3,4] and $LiMnO_2$ electrodes,[5,6] hydrogen in $LaNi_5$,[7] and protons into nickel hydroxide.[8-10] In the latter example, the ''equilibrium potential'' measured during charge (*i.e.*, proton extraction) is 40 to 90 mV higher than that measured during discharge (*i.e.*, proton intercalation) at room temperature.[8-10] The potential offset between charge and discharge decreases approximately 0.5 mV for every 1°C increase in temperature,[8] and at room temperature the offset decreases by 40 mV with the addition of cobalt to the active material.[9,10]

The hysteresis loop generated during a complete charge and discharge reveals that such loops are stable, reproducible, and rate-independent. However, it has been shown in adsorption and magnetism studies that these ''boundary curves'' reveal only limited aspects of the hysteresis phenomenon.[1] Curves generated on partial cycling of the independent variable (*i.e.*, ''scanning curves'') are required to analyze the system completely. To date, no thorough study of the hysteresis in an electrochemical system has been performed.

The purpose of this paper is to gain insight into the hysteresis during the exchange of protons in nickel hydroxide. This is achieved by first measuring and comparing the boundary curves from films of different structure (pure Ni, cobalt doped Ni, and aged films). Subsequently, the ''permanent'' nature of the hysteresis effect in nickel hydroxide is confirmed by conducting experiments as a function of time. Following this, various theories that have been proposed to explain hysteresis are examined, which illustrate the importance of the scanning curves in understanding the material's history dependence. The extent of applicability of these theories to the nickel hydroxide electrode is discussed by comparing them to experimental data. Finally, an empirical approach to predict the scanning curves based on the boundary curves is illustrated. It should be noted that the history or memory that is described in this paper is not the oft described ''memory effect'' in nickel batteries.[11] While the memory effect is exhibited as an inability to discharge fully the electrode after it has been partially discharged repeatedly, the memory in this paper deals with the potential being dependent on the proton intercalation history. The electrodes described here do not exhibit the memory effect seen in nickel batteries.

Equilibrium Potential of the Nickel Electrode

The measurement of the equilibrium potential of the nickel electrode as a function of the state-of-charge (SOC) (z) is complicated by three properties of the material. The first complication arises from the complex nature of the nickel hydroxide redox reaction, which leads to ambiguity in relating the measured potential to the activity of the oxidized and reduced species. The charge and discharge process in the nickel hydroxide electrode involves the extraction and intercalation of protons, respectively, into the solid crystal lattice. Ideally, this has been represented as[12]

$$Ni(OH)_2 \underset{\text{discharge}}{\overset{\text{charge}}{\rightleftarrows}} NiOOH_{2-z} + zH^+ + ze^- \qquad E_{Ni} = 0.29\,V \text{ (in 3\% KOH at } z = 0.5 \text{ } vs. \text{ Ag/AgCl)} \quad [1]$$

Using Reaction 1, previous investigators have defined the standard equilibrium potential as the point where there are equal quantities of Ni^{2+} and Ni^{3+} by assuming that the electrode is a solid solution of $Ni(OH)_2$ and NiOOH.[13-15] Therefore, z is equal to the ratio of Ni^{3+} to the total nickel concentration. The problem with this approach is that Reaction 1 is only an idealized representation of the redox behavior of the electrode, as the material is thought to have Ni^{4+} in the lattice.[16-18] Spectroscopic evidence and chemical analyses suggest that the Ni^{4+} is a consequence of the material's considerable nonstoichiometry (*i.e.*, presence of Ni defects), with some Ni sites occupied by potassium ions or protons in addition to the protons in-

* Electrochemical Society Active Member.
** Electrochemical Society Fellow.
[c] Present address: Department of Mechanical and Nuclear Engineering, Pennsylvania State University, University Park, Pennsylvania 16802.

tercalated in reaction 1.[18] These variations result in the number of electrons transferred per mole of nickel not necessarily being 1.0, as implied by Reaction 1. Rather, this number depends on the change in defect structure during charge or discharge.[19]

The second complication in measuring the equilibrium potential is that the potential measured when the material is charged to 50% of its total capacity ($z = 0.5$) is 40 to 90 mV higher than when it is discharged to that point.[8-10] This hysteresis has often been dismissed when reporting equilibrium potentials. It has been assumed that the potential measured on discharge is the true equilibrium of the system, with the potential on charge representing some unexplained departure from equilibrium.[8,15]

The third complication involves establishing equilibrium conditions. For convenience, low-rate, galvanostatic experiments, where potential losses due to kinetic, mass-transfer, and ohmic effects are negligible, have been used to determine the equilibrium potential as a function of *z*. This approach is convenient because a continuous potential *vs. z* curve can be generated in a single experiment. However, such measurements are complicated in the nickel electrode by the oxygen evolution reaction according to

$$4\ OH^- \rightarrow O_2 + 2H_2O + 4e^- \qquad E_{ox} = 0.22\ V\ (\text{in}\ 3\%\ KOH\ \textit{vs.}\ Ag/AgCl) \qquad [2]$$

Since the equilibrium potential for Reaction 2 is less than that for Reaction 1, oxygen evolution occurs simultaneously with the nickel hydroxide redox reaction under normal operating conditions. This coulombic inefficiency means that not all the current going into, and removed from, the system is that due to Reaction 1. Therefore, experiments designed to track the progress of Reaction 1, by relating current to z, have to account for this reaction. One method of achieving this is to use a mathematical model that corrects for oxygen evolution during the charge or discharge.[9,10,19,20]

The use of a galvanostatic experiment, which results in an oxidation current flowing during charge and a reduction current during discharge, led Timmerman *et al.*[21] to speculate that the potential offset did not arise because of a difference in history associated with charge and discharge, but rather the direction of the current. Their argument was that the Schottky barrier formed between the metal current collector and the semiconducting nickel hydroxide caused the potential offset.[21] This barrier would behave as a rectifier, with a current-invariant potential offset when forward biased. In other words, a constant-potential offset would be established when a charging current is passed, with no effect when a discharging current is passed. The potentiostatic experiments performed by Ta and Newman[9,10] should dispel this theory. They showed that the capacity of the electrode depended on whether it was stepped to the particular potential from the discharged state or from the charged state. For either potential step, only a small oxidation current flowed once steady state was reached, corresponding to Reaction 2. Therefore, they established two different equilibrium conditions that differed only by their past history (*i.e.*, a hysteresis).

Experimental

Films of nickel hydroxide were deposited electrochemically on a 0.2 cm^2 gold substrate sputtered on a quartz crystal using a procedure described in detail elsewhere.[22,23] Cobalt-doped nickel hydroxide films were deposited at room temperature in a bath containing 1.8 M $Ni(NO_3)_2$, 0.175 M $Co(NO_3)_2$, and 0.075 M $NaNO_3$ in a solvent of 50 volume percent (v/o) ethanol using a cathodic current of 1.0 mA (5.0 mA/cm^2). The deposition was conducted for 690 s, which was found to correspond to a film of mass approximately 35 μg (175 μg/cm^2) as measured using an electrochemical quartz-crystal microbalance (EQCM). Films deposited under these conditions were determined to have a nickel to cobalt ratio in the film of 88:12.[24] These films are referred to as fresh Ni-Co films. Films referred to as fresh pure-Ni films were deposited using these same deposition conditions and with solutions of the same composition, but devoid of cobalt.

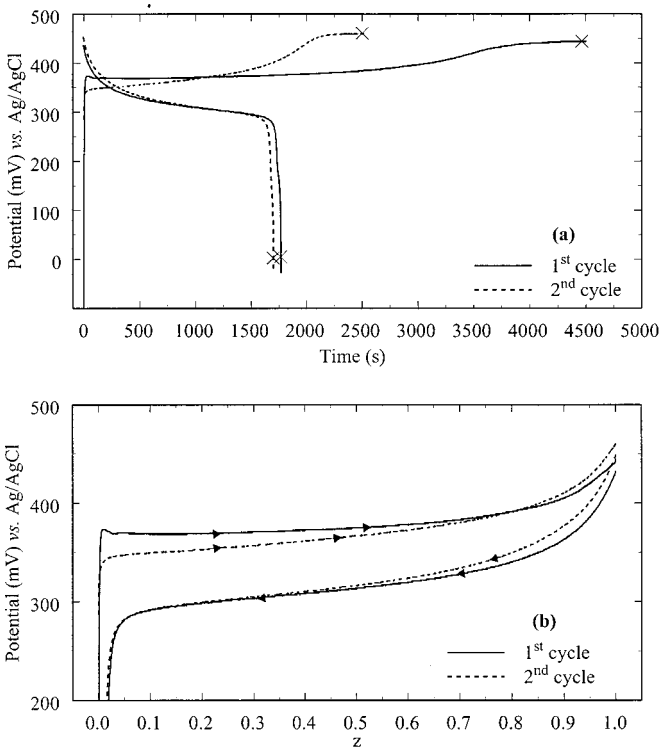

Figure 1. Equilibrium potential of a fresh pure Ni film over the first two cycles generated using a constant current experiment. (a) Shows the significantly greater electron transfer in the first charge. (b) Was generated by converting the abscissa to *z* by correcting 1(a) for the oxygen evolution reaction using Eq. 3-6.

Following the deposition, the films were rinsed in deionized water (resistivity 18.2 MΩ cm), and the cell was filled with a solution of 3 wt % KOH. The films were conditioned by charging at a constant current of 1 mA/cm^2 until oxygen evolution, cycling 25 times at a sweep rate of 5 mV/s between 0.5 and 0.0 V *vs.* Ag/AgCl, and discharging at a constant current of 100 μA/cm^2 until 0.0 V *vs.* Ag/AgCl. Experiments to study the effect of the first charge or the effect of aging in the KOH solution were conducted prior to this conditioning step. Aged films, termed aged Ni-Co films, were prepared by soaking a freshly deposited film in 3% KOH for 40 h. While most experiments were conducted using a three-electrode setup with a platinum counter electrode and a Ag/AgCl reference electrode, experimental sets that were estimated to last more than 5 h were conducted using a Hg/HgO (3% KOH) reference electrode immersed in a Luggin capillary in order to minimize drifts in potential due to the diffusion of OH^- ions into the reference electrode solution. The potentials were then corrected by subtracting 70 mV to match the Ag/AgCl reference electrode. An EG&G M263 A potentiostat/galvanostat was used to perform the experiments. The equipment control and data acquisition were achieved using the M270 software. All constant current experiments reported in this paper were conducted at 100 μA/cm^2. This current density is in a range where the potential of the electrode was current independent.[15] In other words, kinetic, mass-transfer, and ohmic losses are negligible in the curves shown in the paper.

Results and Discussion

Boundary curves for the nickel hydroxide electrode.—Figure 1a shows the first two constant current charges/discharges of a fresh pure-Ni film. The figure illustrates the differing electron transfer that

occurs between the first charge and the subsequent charges/discharges. While the capacity on the first charge (corrected for oxygen evolution) is ≈0.30 C/cm^2, the capacity on the second cycle is only ≈0.18 C/cm^2. This differing capacity is attributed to differences in the exchange of protons and potassium ions from the Ni vacancies between the two cycles.[25] These variations in the structure cause the first charge to show an oxidation state change from 2.0 to 3.67 (a 1.67 electron transfer), while the discharge results in the oxidation state change from 3.67 to 2.67 (a 1.0 electron transfer).[19]

Figure 1a can be rescaled by converting the abscissa from time to z, where z is the SOC defined as

$$z = z^{o} + \frac{Q}{|Q_{max}|} \quad [3]$$

and z^{o} is the value of z at the start of the experiment (*i.e.*, $z^{o} = 0.0$ on charge and 1.0 on discharge). The currents, and hence Q, are positive on charge and negative on discharge. The ratio $Q/|Q_{max}|$ is given by

$$\frac{Q}{|Q_{max}|} = \frac{\int_0^t I_{Ni} dt'}{|\int_0^\tau I_{Ni} dt'|} \quad [4]$$

where τ is the time required to either fully charge or fully discharge the film. These times are indicated by the symbol × in Fig. 1a. Although the total imposed current is constant, the current going to the nickel reaction is not because some of it goes to the oxygen evolution reaction. Therefore

$$I_{Ni} = I - I_{ox} \quad [5]$$

The oxygen evolution reaction varies with voltage, and hence time. Recognizing that the overpotential for the reaction is large, the following Tafel expression is used to describe the process

$$I_{ox} = i_{o,ox} \exp\left(\frac{\alpha_a F(V - E_{ox})}{RT}\right) \quad [6]$$

The parameters in Eq. 6 (*i.e.*, $i_{o,ox}$ and α_a) are obtained by recognizing that on the second charge plateau ($V = 0.443$ V in Fig. 1a), all the current goes to Reaction 2 and none to the nickel reaction. Assuming that $i_{o,ox}$ is more sensitive to the film properties than α_a, the value for the latter parameter obtained from previous work was used (*i.e.*, $\alpha_a = 0.75$)[26], and $i_{o,ox}$ was calculated for each film. This was done by setting $I_{ox} = I$ in Eq. 6, V equal to the potential on the second plateau, and solving for $i_{o,ox}$. This value of $i_{o,ox}$ was then used in Eq. 6 to calculate I_{ox}, and hence, I_{Ni}, as a function of V throughout charge. This value of $i_{o,ox}$ was also used on subsequent discharge boundary curves and scanning curves. When a series of experiments were performed on the same film, the $i_{o,ox}$ was estimated periodically in order to ensure its invariance with cycling.

The procedure detailed above, in conjunction with Eq. 3-6, was used to convert Fig. 1a into a plot of potential *vs.* z as shown in Fig. 1b. The efficiency of the nickel reaction was found to be approximately 67% in the first charge and 73% on the second when charged until the cutoff time, marked by x. The comparable efficiencies during the first two charges mean that the number of coloumbs going to the first charge is nearly 70% more than the second (*i.e.*, the first and second charges give a 1.67 and 1.0 electrons transfer, respectively[19]). The efficiency on discharge was nearly 98%, owing to the lower potential of the discharge boundary curve compared to the charge boundary curve. Adding cobalt to the nickel lattice increases the efficiency, especially on charge, because the voltage is lower.

The most striking effect of rescaling from time to z occurs when comparing the first and second charges. Even though the first charge lasts nearly 70% longer than the second, the curves are very similar to one another when the potential is plotted *vs.* z. In addition, cycling the fresh pure Ni films results in a steady decrease in the number of electrons transferred,[19] but plotting the potential *vs.* z results in overlapping discharge curves.

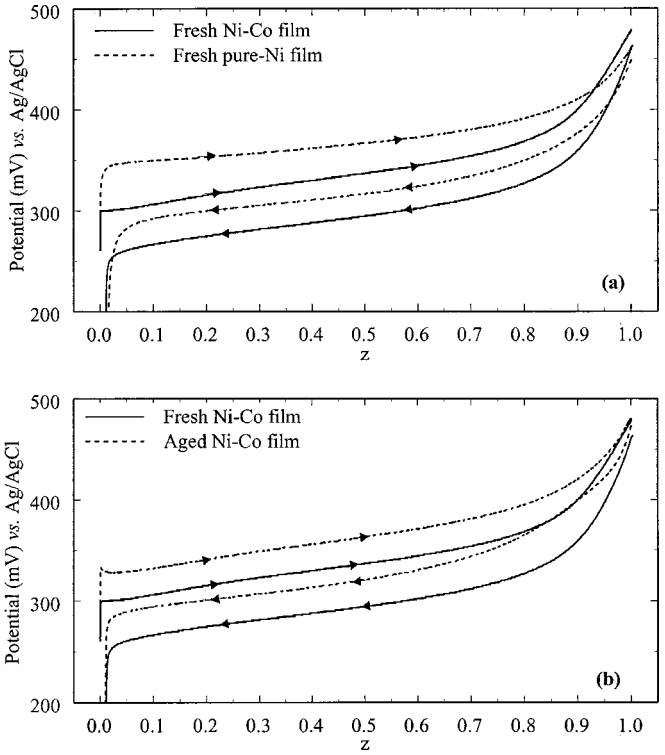

Figure 2. Equilibrium potential *vs.* z for a fresh pure-Ni film and a fresh Ni-Co film (a) and a fresh Ni-Co film and an aged Ni-Co film (b). The film was aged in 3% KOH for 40 h. All curves correspond to the second cycle.

The same qualitative trends seen in Fig. 1a and 1b for fresh pure Ni films are also seen in Fig. 2 for fresh and aged Ni-Co films. However, the potential needed to charge and discharge the electrode does depend on the type of film cycled. Figure 2a shows the second cycle for a fresh pure Ni film compared to the second cycle for a fresh Ni-Co film. The potential of the fresh Ni-Co film is lower,[9,10] and the potential offset between charge and discharge is 53 and 43 mV for the fresh pure-Ni film and fresh Ni-Co film, respectively. In comparison, Ta and Newman[9,10] report an offset of 92 mV for pure Ni films and 50 mV for Co-doped films. The differences may be due to the different film thicknesses employed in the two studies. While the films deposited in this study are estimated to be ≈0.5 μm based on the nickel hydroxide density of 3.5 g/cm^3,[27] Ta and Newman report a thickness of 20 to 40 nm.

A similar shape for the potential *vs.* z curve seen in Fig. 1a and 2a is also obtained when the fresh Ni-Co films are aged in 3% KOH for 40 h as shown in Fig. 2b. Although the potential of the aged film is higher by ≈37 mV, the shape of the curves and the offset between the charge and discharge (43 mV in the fresh film and 45 mV in the aged film at $z = 0.5$) are similar. Spectroscopic studies indicate that aging the film leads to a material with a lower defect content.[28] The lower defect content results in material that cycles between an oxidation state of 2.33 to 3.33, compared to 2.67 and 3.67 oxidation range for fresh material.[25] In summary, the curves in Fig. 1 and 2 show that although the equilibrium potentials depend on the structure of the material, the shape of the curves when plotted against z is similar.

Constant-potential experiments.—Having established the effect of the structure of the active material on the hysteresis boundary curves, we now show that the constant current and constant-potential experiments are comparable. In other words, the hysteresis curves are shown to be independent of what variable is controlled

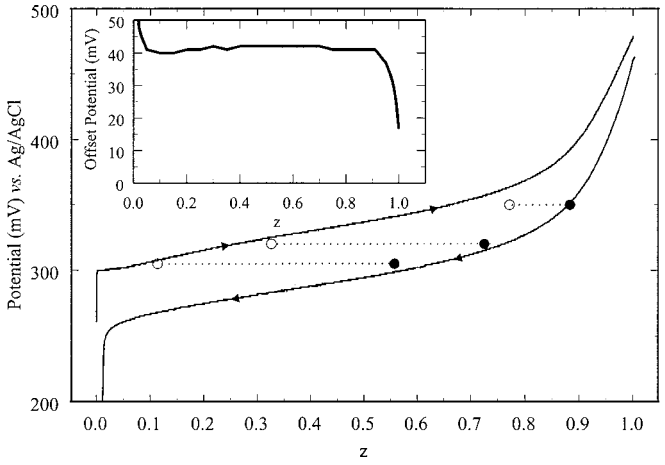

Figure 3. Equilibrium potential *vs. z* for a fresh Ni-Co film. The lines were generated using a constant current experiment and the symbols were generated using a constant potential experiment. The electrode was held at a potential for 1 h, and *z* was determined at the end of the experiment. The solid circles show the data for an electrode initially at the fully charged state, and the open circles are those for electrodes initially at the fully discharged state. The inset plot shows the offset potential as a function of *z*.

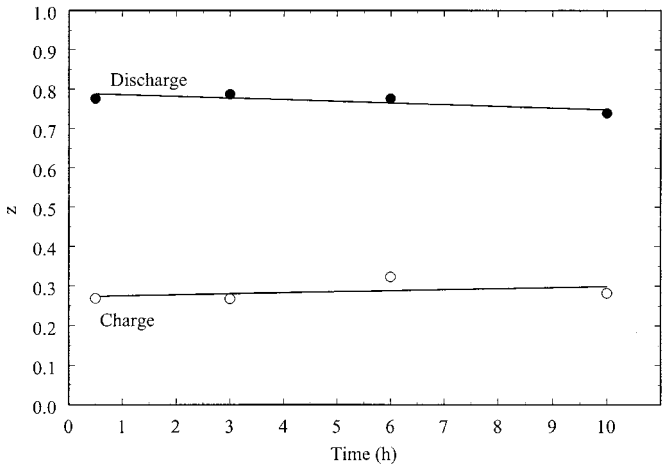

Figure 4. Effect of time on the history-dependent behavior of fresh Ni-Co films. The curves were generated by maintaining the electrode at 319 mV *vs.* Ag/AgCl for different times from the charged and discharged states. The value of *z* was then evaluated by correcting for the oxygen evolution reaction using Eq. 3-6. The curves show that two stable oxidation states can exist at the same potential depending only on the previous history of the electrode.

and independent of the direction of current flowing through the material. Subsequently, we show that the hysteresis is indeed permanent by conducting the experiments as a function of time. All the results shown in the rest of the paper are from fresh Ni-Co films that are conditioned using the procedure described in the experimental section.

Figure 3 shows the experimental equilibrium potential as a function of SOC, *z*, for galvanostatic charge and discharge (denoted by the solid lines). The hysteresis between charge and discharge is also seen in the inset in Fig. 3, where the offset potential is plotted as a function of *z*. The inset shows that the offset is constant through most of the charge/discharge with a value of 43 mV at $z = 0.5$, with the loop closing at $z = 1$. The constant-potential experiment was conducted by first charging the electrode from the completely discharged state to the desired potential, using a constant current, and then holding at that potential for 1 h. The current decayed exponentially to reach a steady-state oxidation current of $\approx 5\ \mu A/cm^2$, corresponding to the oxygen evolution reaction, after approximately 5-10 min. Once this experiment was completed, *z* was determined from Eq. 3 following a galvanostatic discharge to 0.0 V. The resulting *z* and potential are plotted as the open circles in Fig. 3. The constant-potential experiments yield a potential *vs. z* similar to that estimated using the constant current experiments. The highest deviation occurs at the low proton concentrations (circle at $z = 0.75$), where the contribution of the oxygen evolution reaction becomes significant, possibly inducing errors in the estimate of *z*.

The same experiment was repeated during discharge at the three potentials used in the charge. In other words, the electrode was discharged from the completely charged state to the desired potential and then held at that potential for 1 h. Once again, a steady-state oxidation current of $\approx 5\ \mu A/cm^2$ was observed after 5-10 min. The electrode was then discharged to 0.0 V, and *z* was determined from Eq. 3 (denoted by the solid circles in Fig. 3). Again, the constant-potential experiment shows a hysteresis similar to that in a constant current experiment. The results shown in Fig. 3 confirm the conclusion by Ta and Newman that the Schottky barrier cannot be the cause for the hysteresis, as the constant-potential experiment would have resulted in an identical *z*, irrespective of the history of the electrode. In addition, the similarity between the two experiments suggests that determination of the equilibrium state of the system can be achieved by either controlling the current, which is equivalent to controlling *z*, or by controlling the potential.

Further, to confirm that the offset shown in Fig. 1-3 is indeed a permanent hysteresis, the potentiostatic experiments were conducted on a different film where the potential was maintained for various times. Here the electrode was set at a constant-potential on both the charge and discharge for four time periods (1/2, 3, 6, and 10 h), and *z* was determined at the end of each experiment. Figure 4 plots *z* as a function of the time, when the electrode is held at 319 mV *vs.* Ag/AgCl. There is a negligible difference between *z* measured after 1/2 h and that measured after 10 h, on both the charge and discharge. Note that, in the constant current experiment, the whole experiment is completed in ≈1500 s, and yet, Fig. 3 shows that even this short a time is enough to reach equilibrium. Therefore, there exist at least two stable equilibrium states. Which state is achieved is dictated by the history of the material. Furthermore, these equilibrium states can be measured from a convenient galvanostatic charge/discharge experiment.

Domain theory.—The similarity of the hysteresis in nickel hydroxide to those observed in gas/solid adsorption and magnetism leads us to examine domain theory, which has been offered as the description for hysteresis in these systems. For example, experimental evidence suggests that magnetic hysteresis is caused by the loss of energy due to movement of the domain walls, which can be measured in the form of sound intensity (*i.e*, the Barkhausen effect[2]). In this theory, a system that exhibits hysteresis is thought to be made up of a large number of small regions or domains, each of which takes up two or more metastable states for a single value of the external independent variable. The actual cause for the metastability is immaterial at this stage; however, it is important that the domains exhibit such an effect. The metastability in a generic domain was explained by Everett and Whitton[29] in terms of a switch that consists of a bimetallic strip with one end connected to a permanent magnet. The other end of the strip is connected to another permanent magnet through a battery. The magnets are arranged such that, at a temperature T_u, the distance between them reaches a critical value, the contact shuts, and a current flows. On cooling, the circuit is not broken at T_u, but the strip has to be cooled further to T_l where the stress in the strip overcomes the attraction between the magnets. This gives rise to a hysteresis in the system independent of the heating and cooling rate. An analogous example is described here to explain domain theory in nickel hydroxide.

Consider a hypothetical domain of nickel hydroxide, which consists of a finite number of Ni sites, with two interlamellar protons

associated with each site. Analogous to the switch, assume that an interlamellar proton deintercalates from each of the Ni sites at the same potential V_c, whereby the electrode is transformed from the fully discharged to the fully charged state (*i.e.*, z goes from 0 to 1). The resulting potential *vs.* z is plotted in Fig. 5a. However, if some irreversibility were to exist in the domain, such that the proton is reintercalated at a lower potential, for example, V_d, then, hysteresis would occur between intercalation and extraction. This form of irreversibility is comparable to the theory of accommodation described by Everett,[1] where the material is thought to undergo an irreversible step that involves ''prying open'' of the layers of the host material (*e.g.*, NiOOH) to accommodate the guest atom (*e.g.*, H^+).[1] Once intercalation occurs, the expanded solid adopts a new position of minimum energy, so that extraction occurs under a different path. This accommodation effect was proposed by Zheng *et al.*[3] as the cause for the hysteresis during lithium intercalation in hydrogen-containing carbons.[3] They argued that, once intercalation occurs, the lithium binds on the hydrogen-terminating edges of hexagonal carbon fragments, causing a change in the sp^2 bond to an sp^3 bond. Therefore, extraction occurs at a different driving force, hence resulting in hysteresis. The authors assumed that the bonding is an activated process, whereby the hysteresis described in their paper is time dependent. However, the time constants were argued to be long enough such that hysteresis is seen under rates that are experimentally practical.

Another form of metastability in each domain could be due to the occurrence of first-order phase transitions. This approach has been used by Everett and Nordon[30] to explain hysteresis in hydrogen absorbing alloys and has been proposed as a possible cause for the hysteresis in the nickel electrode by Milner and Thomas[8] and Barnard *et al.*[31] Consider a domain in the nickel hydroxide electrode which consists of a solid solution of $Ni(OH)_2$ and NiOOH. Assume the Gibbs free energy of the solid solution has the form depicted by the curve AEGD in Fig. 5b. If the system followed a reversible path, then phase separation would occur at points B and C on charge and discharge, respectively. The resulting potential profile would be ABKCD, and no hysteresis would be observed. However, if on charge the solid solution became supersaturated with NiOOH, the material would be metastable from points B to E. Phase separation would not occur until the potential V_c (*i.e.*, point E), and the charge curve would be AEFD. On discharge, the solid solution could be supersaturated with $Ni(OH)_2$, and the material would be metastable from points C to G. At V_d (*i.e.*, point G), phase separation would occur, and the discharge curve would be DGHA, leading to hysteresis.

There are two discrepancies between the experimental hysteresis curves shown in Fig. 1-3 and the schematics in Fig. 5a and b. Namely, the experimental curves are not horizontal at intermediate z (*i.e.*, the curves are S-shaped), and they are asymmetric (*i.e.*, the potential drops off sharply at z close to 0.0, but it changes more gradually at z close to 1.0). One explanation for these discrepancies can be obtained by considering the electrode to consist of a large number of domains, with each domain consisting of a finite number of Ni sites. Although this explanation applies whether the hysteresis is due to intercalation effects (Fig. 5a) or phase separation (Fig. 5b), the former will be used for illustrative purposes. We assume that the characteristic of each domain is similar to that seen in Fig. 5a, and that each has a critical potential, $V_{c,i}$, where the proton is released from domain i on charge, and a potential, $V_{d,i}$, where the proton reintercalates into domain i on discharge.

If all the domains have the same critical potentials, V_c and V_d, then the boundary curve would be identical to Fig. 5a. Therefore, let us assume that $V_{c,i}$ and $V_{d,i}$ vary among the domains as shown in Fig. 5c. For simplicity, $V_{c,i}$ (shaded circles) and $V_{d,i}$ (open circles) are taken to be normal distributions with the difference between the two potentials, Δ, the same for each domain. The boundary curves can then be constructed by integrating the distribution $V_{c,i}$ and $V_{d,i}$ to give OAB and BCO, respectively, in Fig. 5d. Therefore, even though each domain has a flat potential profile given in Fig. 5a, a distribution of critical potentials where intercalation/extraction occurs results in an S-shaped profile, which more closely resembles the experimental curves. The asymmetry in the experimental boundary curves can be accounted for by having abnormal distribution of domains or by assuming a distribution where Δ varies between the different domains.

In order to generate a scanning curve (*i.e.*, curves generated on partial cycling), the distribution $V_{c,i}$ in Fig. 5c is used until the point A. Integrating this partial distribution yields the forward scan in Fig. 5d (solid line). If the distribution $V_{d,i}$ does not depend on the charge history, then on reversing the direction of the scan the system reverts to the distribution $V_{d,i}$ at the point C. Integrating $V_{d,i}$ from C results in the reverse scanning curve as shown in Fig. 5d. The resulting scanning curve has a vertical line (AC) from the forward path to the reverse path indicating that intermediate potentials cannot be attained at that z. An asymmetric boundary curve would also result in an immediate drop from the charge to the discharge boundary curve as soon as the current is reversed. Ta and Newman[9,10] speculate that the scanning curve for nickel hydroxide would follow such a path.

However, if the discharge distribution changes as the electrode is charged, then the solid $V_{d,i}$ curve is reached only after the electrode is fully charged. When the electrode is charged to $z = 0.5$, the $V_{d,i}$ distribution has only reached the dotted line in Fig. 5c. Reversing the current at this point causes the domains to discharge along a different path from that of the fully charged electrode. A changing distribution suggests that the domains do not act independently, but are dependent on the nature of the surrounding domains. The result is the S-shaped dotted line AO. For the same set of boundary curves, there could be an infinite number of scanning curves, depending on the degree to which the domains interact. Therefore, the scanning curves, not just the boundary curves, are essential to characterize the hysteresis completely. This implies that in electrochemical systems that exhibit hysteresis, the potential cannot be used as a means of estimating the SOC. In addition, relating z to the ratio of the activities of the oxidized and reduced species,[32] and in turn relating them to the potential using Nernstian thermodynamics,[13-15] would not be appropriate for such systems.

Scanning curves for the nickel hydroxide electrode.—Figure 6 shows the boundary curves and the discharge scanning curves for the nickel hydroxide electrode. The boundary curves were generated by correcting the potential-time charge/discharge curves for oxygen evolution as detailed previously. To generate the scanning curves, the electrode was charged until a known amount of coulombs was passed; the current was reversed, and the electrode was discharged to a cutoff potential of 0.0 V. The curves were then converted to potential *vs.* z by correcting for oxygen evolution using

$$z = \frac{|Q_{sc}| + \int_0^t I_{Ni} dt}{|Q_{max}|} \qquad [7]$$

$|Q_{max}|$ is equal to the denominator in Eq. 4, I_{Ni} is given by Eq. 5, and $|Q_{sc}|$ is the capacity of the scanning curve, evaluated using

$$|Q_{sc}| = \left| \int_0^{\tau_{sc}} I_{Ni} dt \right| \qquad [8]$$

where τ_{sc} is the time taken to reach 0.0 V in the scanning curve. Figure 6 shows that the discharge scanning curves lie in the separation between the charge and discharge boundary curves, confirming that states within the hysteresis loop are accessible.

Figure 7 shows the charge scanning curves on the same electrode, where again the existence of the intermediate states is confirmed. The curves were generated by fully charging an electrode from the fully discharged state, following which the electrode was discharged until a known amount of coulombs were passed, and the current reversed. The curves were then corrected for the oxygen evolution reaction using Eq. 3-6 with z^o taken to be the z at the start

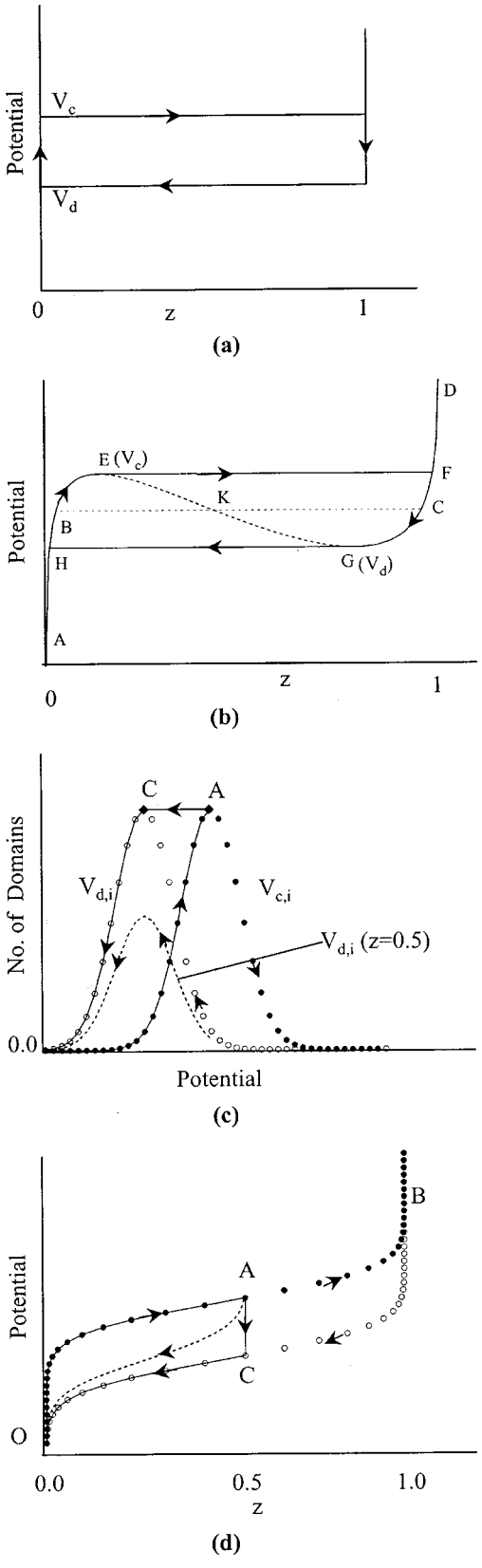

Figure 5. Schematic representation of the domain concept applied to the nickel hydroxide electrode. (a) Shows the boundary curves in a domain which exhibits metastability due to an intercalation effect and (b) due to phase separation. (c) Shows a distribution of the potentials defined in (a) for the different domains, and (d) is the corresponding response of the system. Two possible scanning curves are shown in (c) and (d), one by the solid line, and the other by the dotted line.

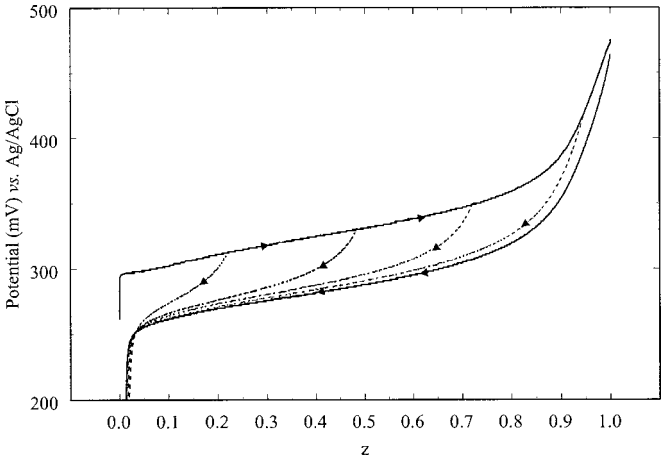

Figure 6. Discharge scanning curves for fresh Ni-Co films. The curves were generated by discharging the electrode after a partial charge. The curves were then converted to *z* by correcting for the oxygen evolution reaction, as detailed in the text, and forcing the end of discharge to occur at $z = 0$.

of the scan and using the discharge boundary curve to evaluate the denominator in Eq. 4. The confidence in the estimate of *z* decreases as $z = 1.0$ (*i.e.*, the fully charged state) is approached, due to the large fraction of oxygen evolution in this region. The shape of the scanning curves in Fig. 6 and 7, when interpreted using domain theory, suggests two aspects of the nature of the domains, namely, (*i*) there is a distribution of critical potentials where metastability occurs over the domains and (*ii*) the behavior of each domain is history dependent within the range of metastability.

Figures 6 and 7 show that small changes in *z* on the boundary curves result in the potential of the material changing to values between the boundary curves. Alternatively, when the potential is the independent variable, this result can be reinterpreted to mean that even small changes in potential within the boundary curves will lead to proton intercalation/extraction (*i.e.*, changes in *z*), with a finite current passing through the system, a result that was observed experimentally. Hence, techniques that involve perturbations of the potential within the boundary curves (*e.g.*, potential step[33-35] and electrochemical impedance spectroscopy[24,36]) would involve intercalation/extraction of protons. This is in contrast to Ta and Newman's speculation that such experiments would have little

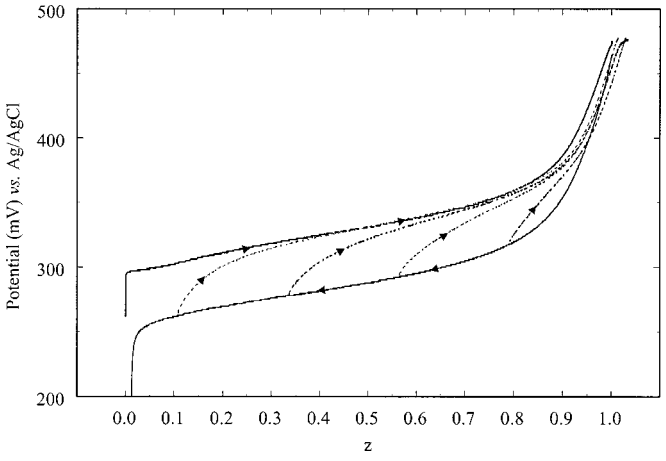

Figure 7. Charge scanning curves for fresh Ni-Co films. The curves were generated by charging the electrode after a partial discharge. The curves were then converted to *z* by correcting for the oxygen evolution reaction, as detailed in the text, and forcing the value of *z* at the start of the charge to correspond to the value of *z* at the end of the previous discharge.

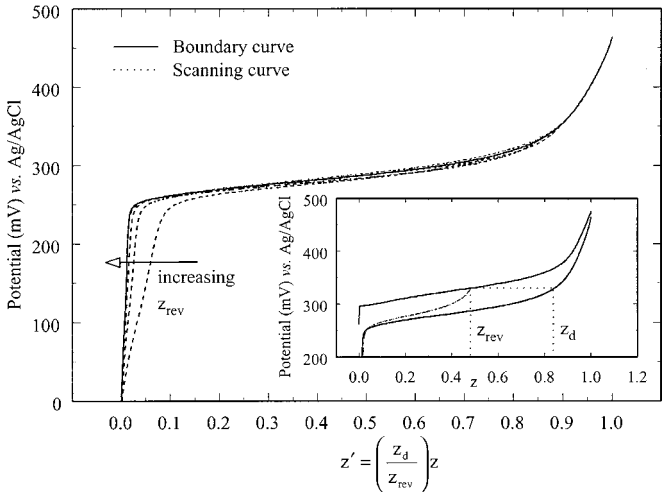

Figure 8. Rescaled discharge scanning curves for fresh Ni-Co films. The rescaling was accomplished by stretching the scanning curves in Figure 6 until they touch the boundary curve as illustrated in the inset.

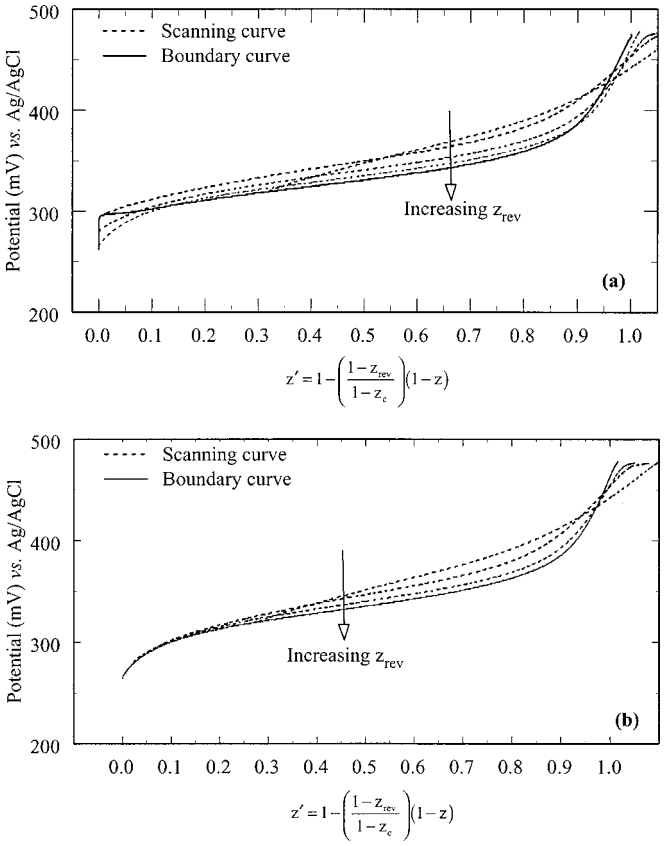

Figure 9. Rescaled charge scanning curves for fresh Ni-Co films. (a) Was normalized by forcing the potential at the start of the scan to lie on the boundary curve. (b) Was generated by forcing it to lie on the longest scanning curve. The solid line indicates the boundary curve, and the dotted lines the scanning curves.

meaning, as the authors assumed that intermediate potentials between the boundary curves would not result in proton intercalation/extraction.[9,10] However, Fig. 6 and 7 show that, at any *z*, the slope of potential *vs. z* on the scanning curve is different from that on the boundary curve. This suggests that the amount of proton intercalated on the positive potential step from the boundary curve would be different from that on a negative step. Therefore, a more detailed understanding of the role of the domains is needed in order to estimate parameters (*e.g.*, diffusion coefficient) based on these perturbation techniques.

Not only are multiple potentials attained at each *z* (*e.g.*, one on the charge, a second on the discharge, and another for each scan), but also a similar S-shape is observed when comparing the boundary curves to the scanning curves, as mentioned previously. The similarity between the boundary and scanning curves is especially striking when the abscissa of the scanning curves are rescaled (Fig. 8 and 9). The rescaling in Fig. 8 is accomplished by stretching each discharge scanning curve in Fig. 6 until it touches the discharge boundary curve. For example, the boundary curves and one of the scanning curves from Fig. 6 are reproduced as an inset in Fig. 8. The figure defines two values of *z*, namely, z_{rev}, denoting the *z* at which the scan is reversed and z_d, denoting the *z* on the discharge boundary curve that has the same potential as does z_{rev}. The abscissa is then rescaled using $z' = (z_d/z_{rev})z$ to generate Fig. 8. Note that for a boundary curve, $z_d = z_{rev}$ and therefore, $z' = z$. Although no physical basis exists for the rescaling, it is seen from Fig. 8 that the scanning curves overlap on the boundary curve, and only the end of the very short scanning curve deviates from the boundary curve.

A similar analysis was undertaken for the charge scanning curves as shown in Fig. 9a, where the scanning curves were rescaled to touch the charge boundary curve using an equivalent procedure by defining a reversal point, z_{rev}, and an equivalent point on the charge curve, z_c. Although the quantitative overlap in Fig. 9a is not as good as in Fig. 8, the qualitative shapes are similar. The major qualitative difference is that the boundary curve has a very sharp rise in potential at the beginning of charge, where the scanning curves show a more gradual increase. This gradual increase is seen even when the current is reversed at the knee at the end of discharge where $z \rightarrow 0$. Only when the discharge is continued until the potential reaches 0.0 V *vs.* Ag/AgCl is the sharp rise in potential at the beginning of charge seen. Hence, the rescaling was changed so that the scanning curves touch the longest charge scanning curve by assuming that it was representative of the charge boundary curve. Again, the reversal point, z_{rev}, and an equivalent point on this charge boundary curve, z_c, were used for the rescaling, which is shown in Fig. 9b. Although, differences are still evident between the scanning curves, the overlap is better than that in Fig. 9a, especially at low values of *z*. It is known that when the nickel hydroxide electrode is completely discharged, the conductivity of the material is very low and the material behaves as a semiconductor.[13] This low conductivity could be the cause for such differences between the boundary and scanning curves.

As mentioned earlier, there can be an infinite number of scanning curves for the same set of boundary curves depending on the distribution of the domains and their interaction with the adjacent domains. However, independent of these interactions, Everett and Smith[37,38] argue that the boundary and scanning curves obey certain theorems. Using various distributions to describe the boundary and scanning curves, Everett and Smith[37,38] outline seven theorems that describe the relationship between the boundary and scanning curves. These theorems also govern the trajectories of the system inside the hysteresis loop. Any system that exhibits a true hysteresis due to the existence of domains should follow theorems 3 to 7 and either theorem 1 or 2. We first describe the theorems in electrochemical terms, and then compare them to the nickel hydroxide electrode to see their applicability. For details of the derivation of the theorems and their limits of applicability see Everett and Smith[37,38] and Enderby.[39,40]

Theorem 1.—If the discharge scanning curves meet the discharge boundary curves before the electrode is fully discharged, then the charge scanning curves will meet the charge boundary curves before the electrode is fully charged. The scanning curve from A to C in Fig. 5d is an extreme case of theorem 1 where the scanning curve meets the boundary curve, but with no change in *z*.

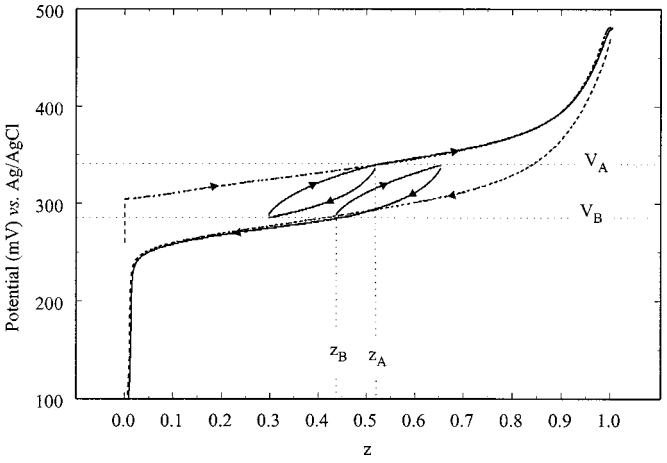

Figure 10. Test of the validity of theorem 4 and 5 for fresh Ni-Co films. The scanning curves were generated by reversing the (constant) current at the potentials shown by the light dotted lines. The left loop starts from charging beginning at $z = 0$, and the right loop starts from discharging beginning at $z = 1$. Note that the system continues along the boundary curve after experiencing one current reversal at V_A (for the initially charging curve). For the initially discharging curve, the first current reversal occurs at V_B and the second at V_A.

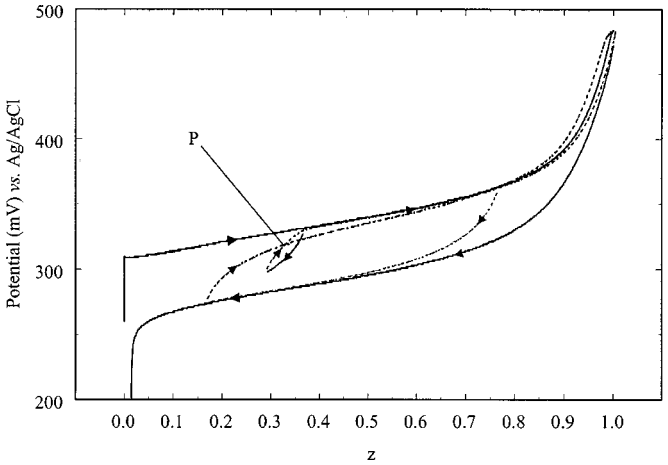

Figure 11. Test of the validity of theorem 6 for fresh Ni-Co films. The curves were generated by cycling the current over two different ranges of z from the charge boundary curve. As predicted by theorem 6, the path of the system after it crosses point P is dependent on its history.

Theorem 2.—If the discharge scanning curves converge on the lower intersection point of the boundary curves ($z = 0$), the charge scanning curve will converge on the upper intersection point ($z = 1$). In other words, the scanning curves meet the boundary curve at $z = 0$ or $z = 1$ only, and not at any intermediate z. The dotted scanning curve from A to O in Fig. 5d corresponds to theorem 2, where the scanning curve meets the boundary curve only at $z = 0$. Figures 6 and 7 reveal that the scanning curves in the nickel hydroxide electrode closely resemble curve AO in Fig. 5d, and therefore, can be said to follow theorem 2.

Theorem 3.—The slope of the discharge scanning curve must always be more than that of the discharge boundary curve at the same z; similarly, the slope of the charge scanning curve should be more than that of the charge boundary curve at the same z. We can see from Fig. 6 and 7 that this is true for the nickel hydroxide electrode.

Theorem 4.—The first part of this theorem predicts that if the path of the system is reversed at a particular potential V_A, with a corresponding $z = z_A$, and the potential scanned to V_B and back to V_A, then z will return to z_A. The experimental data in Fig. 10 show the results as envisioned in this theorem. Here, the electrode was charged from the completely discharged state to $V_A = 335$ mV *vs.* Ag/AgCl, which corresponds to $z_A = 0.52$. The current was reversed to generate a discharge scanning curve until the potential reached $V_B = 285$ mV. The current was reversed again to generate a charge scanning curve, where it returned to the point $V_A = 335$ mV and $z_A = 0.52$ as predicted by the theorem. The second part of this theorem predicts that cycling the potential between V_A and V_B will lead to a loop of constant shape and area independent of the position of z. In order to test this part of the theorem, the electrode was completely charged and then discharged to $V_B = 285$ mV, corresponding to a $z_B = 0.44$. The current was reversed to generate a charge scanning curve until the potential reached $V_A = 335$ mV. The current was again reversed to generate a discharge scanning curve, where it returned to the point $V_B = 285$ mV and $z_B = 0.44$. As predicted, the two scanning loops have the same shape and area. These two internal loops are reproducible, and one can cycle between the points V_A and V_B with negligible change in the shape of the loops. Such reproducible internal loops also have been seen in adsorption hysteresis.[1]

Theorem 5.—If, when the systems returns to V_A as envisioned in theorem 4, z is allowed to increase by continuing the charge, the system will move along the same curve as that which would have been followed if no loop had been traversed from V_A (*i.e.*, on the boundary curve). To test this prediction, the electrode that was used to test for theorem 4 was charged to $z = 1$ after the loop returned to V_A. The resulting potential is also shown in Fig. 10, although it is not evident as it overlaps with the boundary curve. The proximity of the two curves confirms the applicability of this theorem. A similar effect is seen on continuing the discharge past the point V_B to $z = 0$, with the curve approximately overlapping on the discharge boundary curve. Theorem 5 is also called the wiping-out property of a system exhibiting hysteresis, as the memory of the systems excursion at V_A is wiped out as soon as it returns to this point and the system behaves as if there was no excursion at V_A.[41]

Theorem 6.—Any point P within the hysteresis loop can be reached in a number of ways, some from lower z, others from higher. Although the system can be described by its potential and SOC (*i.e.*, V and z), its state will not be completely defined since its behavior when it moves away from P depends on its route by which this point was approached. The importance of this theorem is that the path of the system within the hysteresis loop depends on its history, or in other words, the shape of the scanning curves is related to a history-dependent distribution. This theorem has been the argument behind using the domain concept and is fundamental to the description of the scanning curves.

In addition, experimental evidence of this theorem disproves the theory for hysteresis proposed by Duhem, as described by Everett and Smith.[37] Duhem describes the scanning curves to be one of two families of curves, the ascending series and the descending series, such that only one of each family passes through each point. The ascending curves are the possible paths of the system when the potential is increasing, and the descending curves when the potential is decreasing. This is in contrast to what is described in theorem 6, which states that each point in the loop can be reached by an infinite number of paths. Figure 11 shows experimental data that support theorem 6 and thereby disprove the theory of Duhem in the nickel hydroxide electrode. Here, the electrode was charged using a constant current until $z \approx 0.8$, when the current was reversed to generate a discharge scanning curve until $z \approx 0.15$, at which point the electrode was charged again to complete the loop. The electrode was then completely charged and then discharged, after which a second loop was traversed, but over a shorter z compared to the first, as indicated in the figure. Due to theorem 4, the system tries to return

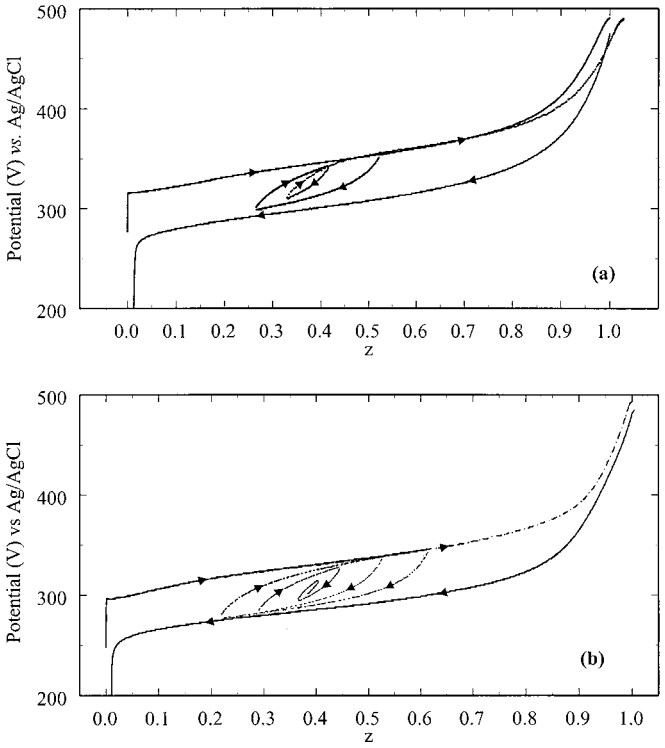

Figure 12. Test of the validity of theorem 7 for fresh Ni-Co films. (a) Was generated by cycling the current over two successively smaller ranges of z from the charge boundary curve. Note that the path of the system after a reversal approaches the point of previous reversal, thereby wiping the history of both the primary and secondary excursion. (b) Illustrates the path of the system when Δz was decreased in each cycle, where the curves appear to approach the midpoint between the boundary curves.

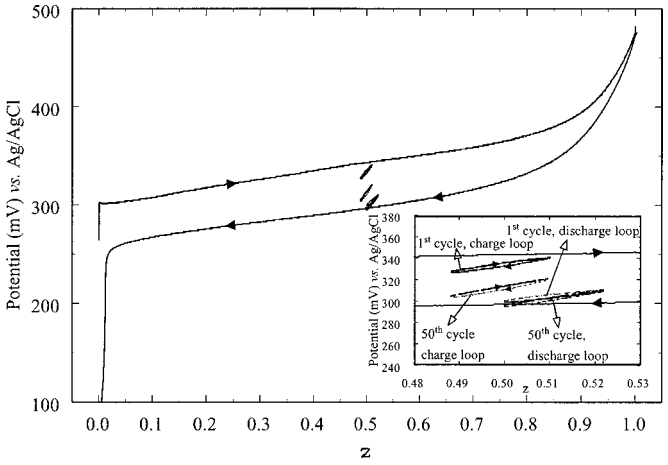

Figure 13. Equilibrium curves measured as a function of cycling over a small range of z. The curves were generated by charging and discharging the electrode using a constant current over a Δz of 0.02 for 50 cycles during charge and discharge. The inset plot shows the drift in potential toward the discharge boundary curve. The time for each charge (or discharge) was 30 s, resulting in the completion of the 50 cycles in 3000 s. In contrast, In Fig. 4, the system was shown to be relatively stable over 10 h.

to the point where the excursion from the main loop began. This property ensures that the charge scanning curve in the shorter loop crosses the one in the longer loop at the point P. Notice that, as predicted by theorem 6, the path of the system beyond point P is different and depends on the route by which the point was reached.[41]

Theorem 7.—If the system is taken through a series of oscillations of Δz of decreasing amplitude, after the nth reversal, the system moves toward the point where the $(n-1)$th reversal occurred; if the system is carried through this point, it moves toward the $(n-3)$rd reversal point, and so on. This theorem is an extension of theorem 4, in that it describes the wiping out of the memory when the system is taken on an excursion on the internal loops. In order to test the validity of this theorem, the system was charged from the completely discharged state until $z \approx 0.55$, at which point the direction was reversed. This discharge scan was maintained until $z \approx 0.25$, when the direction was again reversed, as shown in Fig. 12a. An internal loop to this excursion was executed by reversing this scan at $z \approx 0.4$ and again at $z \approx 0.3$. The system was then allowed to charge completely to $z = 1$. As stated by the theorem, the system returns to the point where the secondary excursion occurred, thereby wiping out the secondary history. Charging the electrode further results in the system wiping out the primary history.

In order to observe the path of the system when Δz was decreased in each cycle, an experiment was conducted as shown in Fig. 12b. Here the system was charged from the completely discharged state until $z \approx 0.6$, at which point the direction was reversed. This discharge scan was maintained until $z \approx 0.2$, when the direction was again reversed. This reversal was continued at successively lower intervals. As seen from Fig. 12b, a reversal results in the curve approaching the previous reversal point, as predicted by the theorem. In addition, the curves appear to approach the midpoint between the boundary curves.

The close agreement of the predictions of these theorems with the experimental data on the nickel electrode leads us to conclude that the nickel hydroxide electrode's behavior is consistent with the existence of a number of individual units or domains, each of which exhibits two or more metastable states. While domain hysteresis is commonly studied in adsorption and magnetism, the effect seems to have been studied in only one electrochemical energy storage system, namely, the $Li/LiMnO_2$ cells. In attempting to explain the production of heat in these cells, Murray *et al.*[5] conclude that a part of the heat is produced by the hysteresis effect. Although, the potential of the material appears to represent that of a "solid solution,"[42] the authors suggest that in reality the material could be exhibiting a first-order phase transition, the signatures of which are modified by the disorder in the material. Therefore, the system can be thought to have domains of coexisting phases. The authors also suggest that the memory of the system is stored in the position of the phase boundary, and movement of the phase boundary causes hysteresis.

In a subsequent paper, Sleigh *et al.*[6] attempt to understand this hysteresis effect by analyzing data on short cycles within the hysteresis loop and comparing their behavior to the general theorems of hysteresis as described above. Loops similar to those shown in Fig. 10, where the electrode is cycled between two points, were generated. However, the authors note that the potential within the loop is parallel to that of the discharge boundary curve, contrary to what is expected in theorem 3. In addition, the graph does not seem to satisfy the wiping-out property that is expected in systems that exhibit domains. Nevertheless, the effect of the history on the material's potential and heat profile is evident, and some similarities are seen with this study.

As mentioned earlier, the material can be made to cycle reproducibly within the hysteresis loop. For example, the loop generated in Fig. 10, where the reversal points touch the boundary curves, can be cycled repeatedly with negligible change in the shape or area. In order to test if the stability is maintained when the loops are small, such that the reversals occur well before the boundary curves, the scanning curves shown in Fig. 13 were obtained. In one set of experiments, a completely discharged film was charged to $z = 0.5$, and then continuously discharged and charged to approximately $z = 0.49$ and 0.51, respectively, 50 times. Similarly, a completely charged film was discharge to $z = 0.5$, and then cycled between z

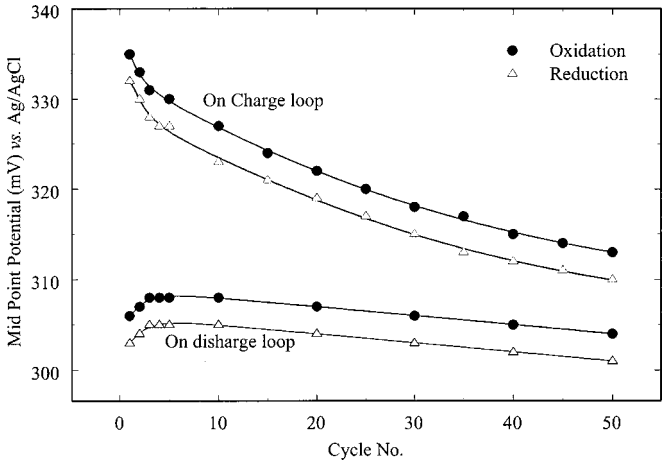

Figure 14. Midpoint potential as a function of cycle number when the electrode is oxidized and reduced over a small range of *z*, as shown in Fig. 13. The plot shows drift in the potential of the curves in the charge boundary curve toward the discharge curve.

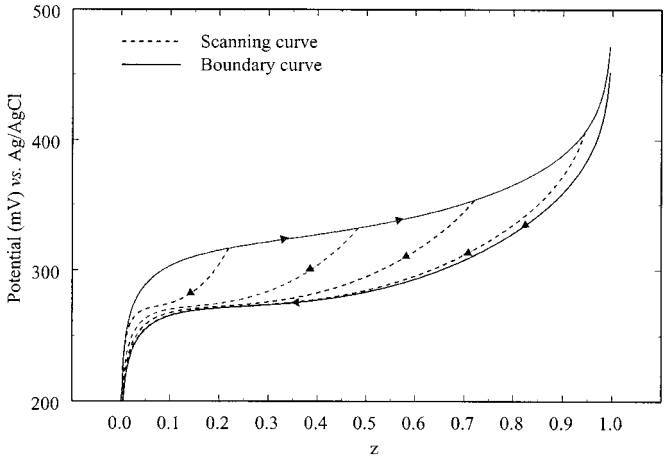

Figure 15. Simulated discharge scanning curves for fresh Ni-Co films. The curves were generated using the procedure outlined in the text. Also shown are the fits of Eq. 9 to the discharge boundary curve and the longest charge scanning curve (solid lines).

$= 0.5$ and 0.52. Figure 13 shows the first and fiftieth loops for these experiments. In Fig. 10, the small loops were not corrected for oxygen evolution as its effect was estimated to be negligible based on Eq. 6. For example, assuming that the side reaction occurs at its maximum rate (*i.e.*, at 343 mV, the potential of the charge boundary curve at $z = 0.5$) over the duration of the 50 cycles, the decrease in *z* is estimated to be less than 3%. Even a 3% change in *z*, though, would result in a decrease in potential of less than 2 mV. Negligible self-discharge was confirmed further by discharging the material at the beginning and end of the 50 cycles, where the capacity removed did not change.

The experiment on charge appears unstable in that the potential of the system decreases until it approaches that of the discharge boundary curve. On the other hand, the cycles on discharge were fairly reproducible, with little change in the potential. This is seen more clearly in Fig. 14, where the potential of the midpoint of the oxidation and reduction experiments are plotted as a function of the cycle number for both the loops (*i.e.*, loops generated after a partial charge and after a partial discharge). The midpoint on oxidation is higher than that on reduction in both cases. This is because extraction occurs at a greater driving force compared to intercalation because of the metastability in the domains. However, the midpoint potentials shift downward as the electrode is cycled. As the *z* at the end of the 50 cycles is the same as that at the start of the experiment, the oxygen evolution reaction can be eliminated as the cause of this drift. This drift is in contrast with the result in Fig. 4, where the system was found to be stable over tens of hours. In addition, it is a deviation from theorem 4, where the potential of the system is expected to return to the same point from where the excursion occurred. While Fig. 12b shows that the system approaches the midpoint between the boundary curves when a few cycles of successively smaller amplitude are imposed, Fig. 13 and 14 show that when numerous small loops of the same amplitude are imposed they approach the discharge boundary curve. This would suggest that the memory of the system's excursion is not completely wiped, resulting in the memory building up over the cycles, thus causing the effect seen in Fig. 13 and 14. The cause for this memory buildup needs to be explored further to understand better the hysteresis in the system.

Empirical procedure to predict the scanning curves from the boundary curves.—Figure 5 illustrates that in order to characterize the hysteresis in a system, the boundary curves alone are not sufficient. That is, scanning curves are needed in order to determine whether the dotted or solid curve results when discharge occurs before the electrode is fully charged. Now that is has been established that the scanning curves follow the form represented by the dotted line in Fig. 5, the boundary curves can be used to predict the scanning curves. Namely, by rescaling the scanning curves, as shown in Fig. 8 and 9, it is possible to collapse the scanning curves on the boundary curves with reasonable accuracy. In the absence of a clear understanding of the underlying phenomenon behind the hysteresis, this empirical approach is used to predict the scanning curves based on the boundary curves. This approach can be used in nickel-based battery models to predict the voltage during partial charge/discharge cycles. The first step in the methodology is to fit the experimental discharge boundary curves to an empirical equation. A nonlinear least-squares package, DataFit, was used to fit Eq. 9 to the discharge boundary curve, with E_{Ni} set equal to *V*

$$E_{Ni} = E^0_{Ni} + \frac{RT}{F}\ln\left(\frac{z'}{1 - z'}\right) + \frac{RT}{2F}[2A_o(1 - 2z') + B_o(1 - 3z'^2)] \qquad [9]$$

The parameters A_o and B_o in Eq. 9 arise from the use of a two-parameter Margules expression to correct for activities.[13-15] In Eq. 9, z' is the normalized *z* used to generate Fig. 8 and 9 and is equal to *z* for the boundary curve. An adequate fit yielded $E^0_{Ni} = 0.2985$ V, $A_o = 3.9745$, and $B_o = -4.6795$. The second step is to identify the point z_{rev} where the scan is reversed and the point z_d on the boundary curve, which has the same potential as the start of the scanning curve (see Fig. 8). For example, the scanning curve originating at 0.48 would yield $z_{rev} = 0.48$ and $z_d = 0.85$. Equation 9 is then used for $0 < z' < 0.85$ to obtain *E*, as shown in Fig. 15. Comparison with Fig. 6 shows that the predictions of the scanning curves are adequate.

A similar procedure can be used to predict the charge scanning curves as shown in Fig. 16. In keeping with the observation in Fig. 9a and b that the shapes of the scanning curves are qualitatively similar to each other but different from that of the boundary curve, the longest charge scanning curve was taken to be representative of the charge boundary curve. A fit of this curve to Eq. 9 yielded $E^0_{Ni} = 0.3398$ V, $A_o = 2.2139$, and $B_o = -2.053$. The subsequent procedure is similar to that described above. While the predictions are adequate at low and intermediate *z*, the deviations are clear as *z* approaches 1. This may be the result of the greater contribution of the oxygen evolution side reaction at high *z*.

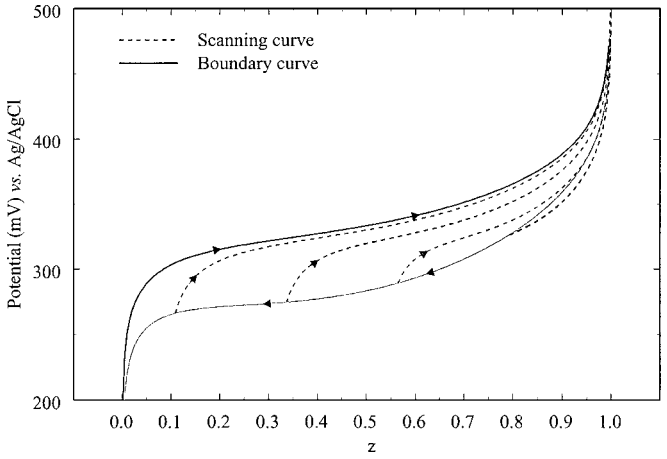

Figure 16. Simulated charge scanning curves for fresh Ni-Co films. The curves were generated using the procedure outlined in the text. Also shown are the fits of Eq. 9 to the discharge boundary curve and the longest charge scanning curve (solid lines).

Conclusions

We confirmed that the nickel hydroxide electrode exhibits a stable hysteresis loop, with the potential on charge being higher than that on discharge at every state-of-charge. We also showed that the charge and discharge potentials vary depending upon the number of electrons transferred (*i.e.*, 1.67 and 1.0), the compositions (pure Ni and Ni-Co), and the defect content, but the shape of the hysteresis loop does not. Furthermore, we showed that the hysteresis loop created during a complete charge and discharge (*i.e.*, boundary curves) is not sufficient to define the state of the system. Rather, internal loops within the boundary curves (*i.e.*, scanning curves) can be generated that access potentials between the boundary curves. The potential obtained at any SOC, as well as how the material charges and discharges from that point, depends on the cycling history of the material.

As little information is available on electrochemical hysteresis, theories proposed in magnetism and adsorption were examined. The theory of domains, where the system is thought to be made up of many small units each of which exhibits two or more metastable states, was found to be applicable in explaining the behavior of the system. The qualitative shape of the boundary and scanning curves suggests that the domains in nickel hydroxide are characterized by two features, namely, (*i*) there is a distribution of critical potentials where metastability occurs over the domains and (*ii*) the behavior of each domain is history dependent within the range of metastability. Although the actual cause for the metastability in each domain is not clear, previous research suggests either energy changes during intercalation or phase separation as possible causes for the phenomenon. The close adherence of the system to the seven theorems outlined by Everett and Smith[37,38] indicates the applicability of domain theory in explaining hysteresis in nickel hydroxide. Although the system follows the path predicted by the theorems closely, deviations from domain theory were seen when the electrode was cycled using a constant current over a small Δz for over 50 cycles. The potential of the electrode was seen to shift from the charge boundary curve to the discharge boundary curve, in deviation from what is expected from theorem 4. This suggests that the experiment did not result in the complete wiping out of the system's memory.

Based on the observation that intermediate potentials between the boundary curves can be obtained by partial charging or discharging (*i.e.*, scanning curves), an empirical procedure was developed to predict the scanning curves based on the boundary curves. The procedure was shown to be adequate to predict the discharge scanning curves, but yielded only qualitative agreement in predicting the charge scanning curves.

Acknowledgments

The authors gratefully acknowledge the financial support from the Office of Research and Development of the United States Central Intelligence Agency, the U.S. Department of Energy under cooperative agreement no. DE-FCO2-91ER75666, and the U.S. Department of Defense under grant no. DAAH04-96-1-0421. Discussions with Professor James Ritter and Michael Matthews (University of South Carolina) on adsorption hysteresis and phase separations are gratefully acknowledged.

The University of South Carolina assisted in meeting the publication costs of this article.

List of Symbols

A_o, B_o, E^0_{Ni}	constants in Eq. 9
E_{Ni}	equilibrium potential for the nickel reaction, V
E_{ox}	equilibrium potential for the oxygen evolution reaction, V
F	Faradays constant, 96487 C/equiv
I	total impressed current, A
I_{Ni}	current to the nickel reaction, A
I_{ox}	current to the oxygen evolution reaction, A
$i_{o,ox}$	exchange current for the oxygen evolution reaction, A
R	universal gas constant, 8.314 J/Kmol
Q	coulombs exchanged to the nickel reaction, C
$\|Q_{max}\|$	absolute value of coulombs exchanged to the Ni reaction, C
$\|Q_{sc}\|$	absolute capacity of the scanning curve, C
z	state-of-charge (SOC)
z^o	SOC at the start of an experiment
z_c	SOC on the charge boundary curve
z_d	SOC on the discharge boundary
z_{rev}	SOC at which the scan is reversed
z'	normalized SOC ($z' = (z_d/z_{rev})z$ for discharge scanning curves and $z' = (1 - z)(1 - z_{rev})/(1 - z_c)$ for charge scanning curves)
T	temperature, K
t	time, s
V	measured voltage *vs.* Ag/AgCl, V

Greek

α_a	anodic transfer coefficient
τ	time required to fully charge or discharge the nickel electrode, s
τ_{sc}	time required to reach 0.0 V for a discharge scanning curve, s

References

1. D. H. Everett, *The Solid-Gas Interface*, E. A. Flood, Editor, Edward Arnold Ltd., London (1967).
2. R. P. Feynman, R. B. Leighton, and M. Sands, *The Feynman Lectures on Physics II*, Addison-Wesley (1964).
3. T. Zheng, W. R. McKinnon, and J. R. Dahn, *J. Electrochem. Soc.*, **143**, 2137 (1996).
4. M. Inaba, M. Fujikawa, T. Abe, and Z. Ogumi, *J. Electrochem. Soc.*, **147**, 4008 (2000).
5. J. J. Murray, A. K. Sleigh, and W. R. McKinnon, *Electrochim. Acta*, **36**, 489 (1991).
6. A. K. Sleigh, J. J. Murray, and W. R. McKinnon, *Electrochim. Acta*, **36**, 1469 (1991).
7. J. J. G. Willems, *Philips J. Res.*, **35**, Suppl. 1, p. 20 (1984).
8. P. C. Milner and U. B. Thomas, *The Nickel Cadmium Cell, Advances in Electrochemistry and Electrochemical Engineering*, C. W. Tobias, Editor, Interscience Publishers, New York (1967).
9. K. P. Ta, Ph.D. Dissertation, University of California, Berkeley CA (1997).
10. K. P. Ta and J. Newman, *J. Electrochem. Soc.*, **146**, 2769 (1999).
11. D. Linden, *Handbook of Batteries*, -2nd ed. McGraw Hill Inc., New York (1994).
12. H. Bode, K. Dehmelt, and J. Witte, *Electrochim. Acta*, **11**, 1079 (1966).
13. P. Barnard, C. F. Randell, and F. L. Tye, *J. Appl. Electrochem.*, **10**, 127 (1980).
14. D. Fan and R. E. White, *J. Electrochem. Soc.*, **138**, 2952 (1991).
15. M. Jain, A. L. Elmore, M. A. Matthews, and J. W. Weidner, *Electrochim. Acta*, **43**, 2649 (1998).
16. A. N. Mansour, C. A. Melenders, and J. Wong, *J. Electrochem. Soc.*, **145**, 1121 (1998).
17. W. E. O'Grady, K. I. Pandya, K. E. Swider, and D. A. Corrigan, *J. Electrochem. Soc.*, **143**, 1613 (1996).
18. Z. Xu, B. C. Cornilsen, and G. Meitzner, *Selected Battery Topics*, G. Halpert, M. L. Gopikanth, K. M. Abraham, W. R. Cieslak, and W. A. Adams, Editors, PV 98-15, p. 1, The Electrochemical Society Proceedings Series, Pennington, NJ (1999).
19. V. Srinivasan, B. C. Cornilsen, and J. W. Weidner, *Selected Battery Topics*, G. Halpert, M. L. Gopikanth, K. M. Abraham, W. R. Cieslak, and W. A. Adams, Editors, PV 98-15, p. 31, The Electrochemical Society Proceedings Series, Pennington, NJ (1999).
20. R. Darling and J. Newman, *J. Electrochem. Soc.*, **145**, 990 (1998).
21. P. Timmerman, B. V. Ratnakumar, and S. Di Stefano, *Aqueous Batteries*, P. D.

Bennet and S. Gross, Editors, PV 96-16, p. 130, The Electrochemical Society Proceedings Series, Pennington, NJ (1996).
22. C. C. Streinz, S. Motupally, and J. W. Weidner, *J. Electrochem. Soc.*, **142**, 4051 (1995).
23. C. C. Streinz, A. P. Hartman, S. Motupally, and J. W. Weidner, *J. Electrochem. Soc.*, **142**, 1084 (1995).
24. S. Motupally, C. C. Streinz, and J. W. Weidner, *J. Electrochem. Soc.*, **142**, 1401 (1995).
25. B. C. Cornilsen, *Selected Battery Topics*, G. Halpert, M. L. Gopikanth, K. M. Abraham, W. R. Cieslak, and W. A. Adams, Editors, PV 98-15, p. 23, The Electrochemical Society Proceedings Series, Pennington, NJ (1999).
26. M. Jain, S. Motupally, and J. W. Weidner, *Aqueous Batteries*, P. D. Bennet and S. Gross, Editors, 96-16, p. 121, The Electrochemical Society Proceedings Series, Pennington, NJ (1996).
27. A. H. Zimmerman and P. K. Effa, Abstract 28, p. 43, The Electrochemical Society Extended Abstracts, Vol. 85-2, Las Vegas, NV, Oct 13-18, 1985.
28. P. L. Loyselle, P. J. Karjala, and B. C. Cornilsen, *Electrochemical and Thermal Modeling of Battery, Fuel Cell and Photoenergy Conversion Systems*, R. J. Selman and H. C. Maru, Editors, PV 86-12, p. 114, The Electrochemical Society Proceedings Series, Pennington, NJ (1986).
29. D. H. Everett and W. I. Whitton, *Trans. Faraday Soc.*, **48**, 749 (1952).
30. D. H. Everett and P. Nordon, *Proc. R. Soc. London, Ser. A*, **259**, 341 (1960).
31. R. Barnard, C. F. Randell, and F. L. Tye, *Power Sources 8*, J. Thompson, Editor, Academic Press, London (1981).
32. A. J. Bard and L. R. Faulkner, *Electrochemical Methods: Fundamentals and Applications*, 1st ed., John Wiley and Sons Inc., New York (1980).
33. G. W. D. Briggs and P. R. Snodin, *Electrochim. Acta*, **27**, 565 (1982).
34. C. Zhang and S. Park, *J. Electrochem. Soc.*, **134**, 2966 (1987).
35. D. Fan, Ph.D. Dissertation, Texas A&M University, College Station, TX (1991).
36. S. Motupally, M.S. Thesis, University of South Carolina, Columbia, SC (1994).
37. D. H. Everett and H. W. Smith, *Trans. Faraday Soc.*, **50**, 187 (1954).
38. D. H. Everett, *Trans. Faraday Soc.*, **50**, 1077 (1954).
39. J. A. Enderby, *Trans. Faraday Soc.*, **51**, 835 (1955).
40. J. A. Enderby, *Trans. Faraday Soc.*, **52**, 106 (1956).
41. J. P. Sethna, K. Dahmen, S. Kartha, J. A. Krumhansl, B. W. Roberts, and J. D. Shore, *Phys. Rev. Lett.*, **70**, 3347 (1993).
42. W. R. McKinnon, J. R. Dahn, J. J. Murray, R. R. Hearing, R. S. McMillan, and A. H. Rivers-Bowerman, *J. Phys. Chem.*, **19**, 5135 (1986).